AUT Journal of Mechanical Engineering

AUT J. Mech. Eng., 7(4) (2023) 419-438
DOI: 10.22060/ajme.2024.23057.6099

The Effect of Turbine Blade Erosion on the Gas Path Measurements and Performance of Micro Gas Turbines

Seyyed Saleh Talebi, Abolghasem Mesgarpoor Tousi* , Ali Madadi

Department of Aerospace Engineering, Amirkabir University of Technology, Tehran, Iran

ABSTRACT: This research aims to find suitable measurements to detect the occurrence of turbine erosion in Micro Gas Turbine engines. For this purpose, the off-design operation of this engine under the turbine's normal and eroded conditions has been modeled and the behavior of different parameters of the gas path has been analyzed. Turbine erosion is one of the most popular issues in gas turbine performance degradation. Accordingly, to have proportional health condition monitoring and diagnostics, it is necessary to know the effects of turbine erosion. Characteristic curves of an eroded turbine is utilized by the proposed off-design model to find the best parameters to detect turbine erosion. In the course of this research, two operation scenarios, one with maintaining the output power and the other with maintaining turbine inlet temperature, are examined. In both scenarios, the running line shifts to a new location with higher airflow and lower pressure ratio. When turbine inlet temperature is maintained, fuel flow, pressure ratio, and output power fall dramatically (9.8%, 11.1%, and 14.3% respectively) while in the other scenario temperature in the combustion chamber inlet and the turbine exhaust with 7% and 7.6% rise and pressure ratio with 4.4% reduction show most deviations from the healthy condition. So depending on the control scenario, the proper parameters can be selected from these sensitive parameters to detect turbine erosion in the Micro Gas Turbine.

Review History:

Received: Mar. 27, 2024
Revised: Jun. 17, 2024
Accepted: Jul. 05, 2024
Available Online: Jul. 12, 2024

Keywords:

Micro Gas Turbine (MGT)
Performance Deterioration
Turbine Erosion
Predictive Maintenance
Gas Path Analysis (GPA)

1- Introduction

Population rise, energy demand growth, limited nonrenewable sources of energy, fuel cost fluctuation, the environment changes, global issues on greenhouse gases, and air pollution rise have attracted a great deal of attention to generate energy through systems with a higher level of efficiency and a lower level of environmental pollution [1, 2]. Distributed Generation (DG) is a solution used extensively to achieve this goal. It is expected that DGs play a vital role in future power generation [3, 4]. In the last decade, micro gas turbines (MGT) have attracted a lot of interest in the area of DG and Combined Heat and Power (CHP) Generation [5, 6]. MGTs are also widely used as a backup of variable renewables in smart grids [7]. Compared with the internal combustion chamber engines (as other choices for DGs), MGT has several advantages such as lower NOx pollution, lower vibration, lower operation and maintenance costs, higher reliability, higher availability, fuel flexibility, and lower required space to install [8]. In addition to the mentioned advantages, the drawback of MGT is its lower electrical efficiency [8]. The electrical efficiency of MGTs is between 28 to 34 percent, while in internal combustion engines, this factor varies between 30 to 40 percent. Using MGTs in DG prepares conditions to utilize exhaust heat and improve overall heat efficiency by over 80%. As heat demands include a considerable part of required energy (for example, in the European Union, this portion is about 50% [9]), utilization of MGT in the CHP cycle covers drawback of relative lower electrical efficiency [8].

Usually, gas turbine components experience difficult operating conditions. Air contaminant such as ash, salt, and water droplets as well as high temperature of turbine blades are some sources that may lead to a degradation of gas turbine components [10, 11]. Fouling and erosion are the main reasons for the performance deterioration of industrial gas turbines [12, 13]. Compressor and turbine damages not only lead to engine efficiency drop but also reduce the engine's safe operation area which may result in engine operational instability. The engine failure imposes considerable costs on engine employers.

Blade erosion is the removal of material from the blade surface due to the impact of hard particles [14]. This phenomenon appears as an increase in surface roughness, reduction in blade thickness, reduction in blade chord, and blunting in blade leading edge [15]. Generally, particles that cause erosion should be larger than 10μm in diameter. Smaller particles tend to track the flow path and only may deposit on the blade's surface and result in blade fouling [14, 16].

*Corresponding author's email: tousi@aut.ac.ir

As today's proper inlet filtration can filter larger particles, usually compressor erosion in industrial gas turbines rarely occurs, but due to fuel impurities, turbine erosion is still a common phenomenon.

Condition-based maintenance is a cost-effective method to improve maintenance strategy and to replace the traditional fail and fix method with predict and prevent approach, which also increases the system's reliability [14, 17, 18]. Non-performance-based monitoring, such as residual oil analysis, and vibration analysis, and performance-based monitoring, such as compressor discharge temperature and pressure monitoring, are counted as some of the monitoring methods.

In the mentioned method, gas path parameters are measured. The measurement deviations from the normal condition are correlated to probable gas path degradation factors using analytical methods such as linear and nonlinear Gas Path Analysis (GPA) and/or artificial intelligence (AI) based diagnostics and prognostics systems. Diagnostics and prognostics are able to present a good estimation of the health condition and the remaining useful life, which leads to maintenance and repair costs reduction and reliability rise [19, 20].

Simulation of component degradations to attain deteriorated performance of component and also related effects on engine performance is an essential and common way to understand the relation between the degradation factor and its signature, which helps to improve and tune monitoring, diagnostic, and prognostic systems [6]. In recent years, several studies on gas turbine component degradation have been published.

In Ref. [21], full and part load performance deterioration of a three-shaft industrial gas turbine is investigated. The degraded map of gas turbine components is calculated through the modification of the clean components map. This simulation shows that the gas turbine performance is not only a function of degradation intensity but also varies with the operating condition and degradation location. Amare et al. [22] modeled the compressor fouling and the turbine erosion using scaling factors and studied related effects on the performance of a double-shaft industrial engine. The results showed that compressor discharge pressure and turbine exhaust temperature show the most deviations against the examined faults. In Ref. [23] the effect of geometric changes on component characteristics is studied by applying a three-dimensional simulation, and a model of gas path diagnosis is established with the change in blade thickness and roughness. The results show the proper capability of the proposed approach for gas path fault detection. In Ref. [24] a fault diagnostic system is presented to detect and isolate the fouling and erosion of a large gas turbine on the basis of a bank of online sequential extreme learning machines.

Although numerous papers have been published in the field of axial turbomachines, there are limited publications about radial inflow ones [25]. In Ref. [26] the effect of component degradation of a MGT is calculated by means of modification factors, and the resulting map is utilized to develop a diagnostic system for the cycle. Talebi and Tousi [27] investigate the effect of radial inflow compressor fouling on the performance of a MGT. This research showed that the combustion chamber inlet temperature is the most sensitive parameter to compressor fouling and the best parameter to detect it.

In Ref. [28], the performance deviation of an MGT under gas path components degradation was investigated. Based on the result analysis, a pattern of parameter behavior was proposed that makes it possible to detect and isolate MGT gas path faults. However, in that research, scaling factors were used to approximate MGT component degradation. In Ref. [29] effect of blade erosion on the performance characteristic of a radial turbine is investigated. In this research, geometry changes due to erosion in three different levels are calculated, and then three-dimensional flow field simulation has been employed to achieve the characteristic map of the eroded turbine.

The simulation of turbine erosion using computational fluid dynamics (CFD) is a time-consuming process and imposes high costs, which can provide beneficial information around turbine deterioration, but the main subject is understanding its effects on the MGT engine performance.

As previously mentioned, fouling and erosion are the most important factors in the gas turbine performance deterioration. The effect of compressor fouling on the MGT performance is investigated in the previous study [27] by the authors. So this research has been performed to complement the mentioned studies ([27, 29]).

For this purpose, an optimum design point of a MGT is determined using governing equations so that it can be set by the turbine that was analyzed in ref [29]. Then a model is proposed to simulate MGT off-design operation. The model is validated against available experimental data of a commercial MGT. Full and part load operation of the engine is modeled in three different levels of turbine erosion. The relative deviations of different parameters are calculated. Finally, parameters with the most sensitivities to the turbine erosion are discovered which can be used as turbine erosion detectors in the online performance monitoring.

As reviewed previously, several studies have been conducted in the area of gas turbine deterioration. Nevertheless, the commercial MGT, as a newly developed technology, has some different features in comparison to the conventional gas turbine, which may result in different behavior against component damage, as shown in [27, 30]. variable speed operating line, recuperative cycle, and using radial inflow compressor and turbine are the essential and significant differences of MGTs versus conventional industrial gas turbines. So some specific study on the MGT would be necessary to find out its behavior against component deterioration. Understanding MGT behavior in case of different damages helps decrease the number of health monitoring sensors and increase the speed and accuracy of diagnostic and prognostic systems. It also helps reduce the operating and maintenance costs of MGT.

Limited researches have been conducted on performance degradation in MGTs. However, due to the lack of a

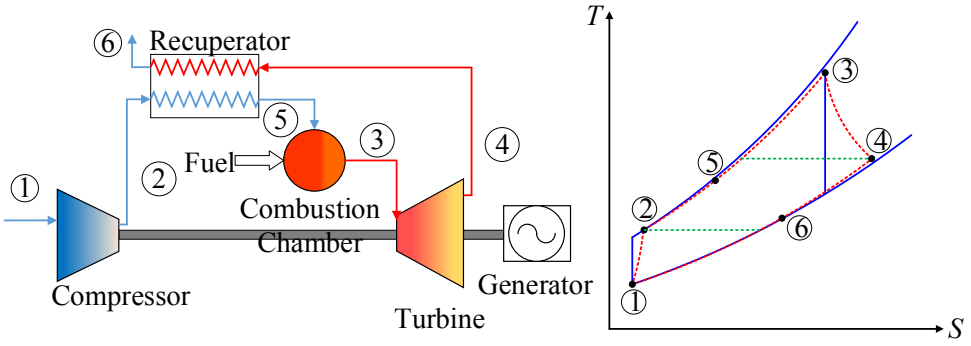

Fig. 1. Schematic diagram of the Micro Gas Turbine

characteristic map of the damaged components, researchers have used the scaling factors to attain a damaged component map to model off-design performance. The advantage of the current investigation is utilizing the characteristics of an eroded turbine gained by a three-dimensional simulation.

In this study, at first, a brief description of MGT components and configuration and design point equations have been presented in section 2. A model is proposed to predict the MGT off-design operation in section 3. Then a validation of off-design simulation and an analysis of the deteriorated behavior of MGT are presented in section 4 followed by a conclusion and remarks in section 5.

The importance and originality of this research are:

- Performance deterioration of a variable-speed recuperated MGT under turbine erosion is modeled and analyzed.
- Characteristic curves of an eroded turbine from a three-dimensional simulation study are utilized.
- Variations of the burner and recuperator performance in part-load operation are taken into account.
- The sensitivity of the gas path and performance parameters to turbine erosion are evaluated.
- The best measurements for early detection of turbine erosion are determined

2- Evaluation of the MGT Design Point Performance

The schematic layout and T-s diagram of the MGT are presented in **Fig. 1**; the main components of the MGT are shown in the figure. A compressor, recuperator, combustion chamber, turbine, and generator are the main components of an MGT. The compressor pressure ratio is low in this engine type, while the gas turbine

exhaust gas temperature (TET) is high enough, which can be recovered to raising the compressor exit air temperature prior to the combustion chamber. This leads to a reduction in the required fuel flow, which can increase in the thermal efficiency of the cycle [31].

The compressor's required power can be expressed as Eq. (1) [32].

$$W_c = \dot{m} \cdot Cp_a \cdot \frac{T_{o1}}{\eta_c} \cdot \left[\left(\frac{P_{o2}}{P_{o1}} \right)^{\frac{\gamma_a - 1}{\gamma_a}} - 1 \right] \quad (1)$$

Where w is specific power consumption, Cp is Heat Capacity, T_o is inlet total temperature, η is isentropic efficiency, P_o is total pressure, and γ is Heat Capacity Ratio.

Eq. (2) denotes the recuperator effect on the cycle [33]. Where ε is recuperator effectiveness.

$$T_{o5} = \varepsilon \cdot \left(T_{o4} - T_{o2} \right) + T_{o2} \quad (2)$$

The ideal fuel mass flow can be determined by Eq. (3) [34]. In which is mass flow rate and LHV is fuel lower heating value. The fuel used in the simulation is liquid octane with an LHV of 45000 kJ/kg.

$$\frac{\dot{m}_f}{\dot{m}_a} = \frac{Cp_g.T_{o3} - Cp_a.T_{o5}}{LHV + Cp_f.T_{o1} - Cp_g.T_{o3}} \quad (3)$$

The turbine output power can be computed through Eq. (4) [32].

$$W_t = \dot{m} \cdot C_{pg} . \eta_t . T_{o3} . \left[1 - \left(\frac{P_{o4}}{P_{o3}} \right)^{\frac{\gamma_g - 1}{\gamma_g}} \right] \quad (4)$$

The design point data of the engine considered in the present study compared to the commercial models available in the market is shown in **Table 1**.

Table 1. Present research selected design point against some commercial MGTs

model	T100 [36-38]	C30 [39, 40]	C60 [38, 39]	C600 [41]	TA100 [38, 42]	Micro-cog [43]	250 sm [38]	current study
Manufacturer	Turbec	Capstone	Capstone	Capstone	Elliot Energy Systems	Ansaldo	Ingersoll Rand Power works	-
Power output (kw)	105	30	60	600	100	110	250	640
Thermal efficiency	30%	29%	28%	33%	30%	34%	32%	36.9%
Pressure ratio	4.5	3.6	4.8	-	4	3.9	-	4.815
Speed (rpm)	70000	96000	96000	-	68000	64000	-	50000
TIT (K)	1223	1117	1225	-	1143	1223	-	1223
Air mass flow rate (kg/s)	0.8	-	0.49	4	-	0.8	-	2.95
Fuel mass flow rate(kg/s)	0.007	-	-	-	-	0.00695	-	0.0385

3- Off-Design performance prediction of the MGT

Variation in demand power from MGT, specifically when used as renewable energy backup, is unavoidable. Consequently, MGT must deal with several changes in operating points every day, which imposes the necessity of knowing part-load behavior. As is shown in the previous section, turbine and compressor power are functions of the mass flow, pressure ratio, and isentropic efficiency of these components. Because of the turbomachinery, these parameters are connected together and to rotational speed. Any change in each of these parameters induces a change to other parameters. The relation between these parameters is known as the component characteristics.

So the analysis of the off-design behavior of MGT is more critical compared to the design point condition while it faces a higher degree of difficulty and complexity [35]. A customary way to calculate the gas turbine performance in an off-design manner is the "zero-dimensional" method.

In this approach, a set of equations is employed to simulate engine behavior. These equations set comprises all components' characteristics equations and compatibility equations that arise from the constraints that

induced due to component mechanical and aerodynamic connection. Hereafter, these equations are introduced.

3- 1- Compressor operation

The compressor's operating characteristics express the correlation between the compressor's performance parameters. These parameters are "corrected mass flow", "pressure ratio", "isentropic efficiency", and "corrected speed" and have been presented in Eqs. (5) - (8)[33, 44].

$$WAC_C = \dot{m}\sqrt{T_{o1}/T_s}\,/\left(P_{o1}/P_s\right) \tag{5}$$

$$N_{cor,c} = N/\sqrt{T_{o1}} \tag{6}$$

$$\eta_c = \left(T_{o2}^s - T_{o1}\right)/\left(T_{o2} - T_{o1}\right) \tag{7}$$

$$PR_c = P_{o2}/P_{o1} \tag{8}$$

Where *WAC* is corrected mass flow and *N* is shaft rotational speed. The standard pressure and standard temperature are 100 kPa and 288 K, respectively. Compressor operating characteristic in this research is derived from [27] and shown in Fig. 2.

3- 2- Turbine operation

The turbine's operating characteristics express the correlation between the turbine's performance parameters. These parameters are "corrected mass flow", "pressure ratio", "isentropic efficiency", and "corrected speed" and have been presented in Eqs. (9) - (12) [33].

$$WAC_t = \dot{m}_g \frac{\sqrt{T_{o3}/T_s}}{P_{o3}/P_s} \tag{9}$$

$$N_{cor,t} = N/\sqrt{T_{o3}} \tag{10}$$

$$\eta_t = \left(T_{o3} - T_{o4}\right)/\left(T_{o3} - T_{o4}^s\right) \tag{11}$$

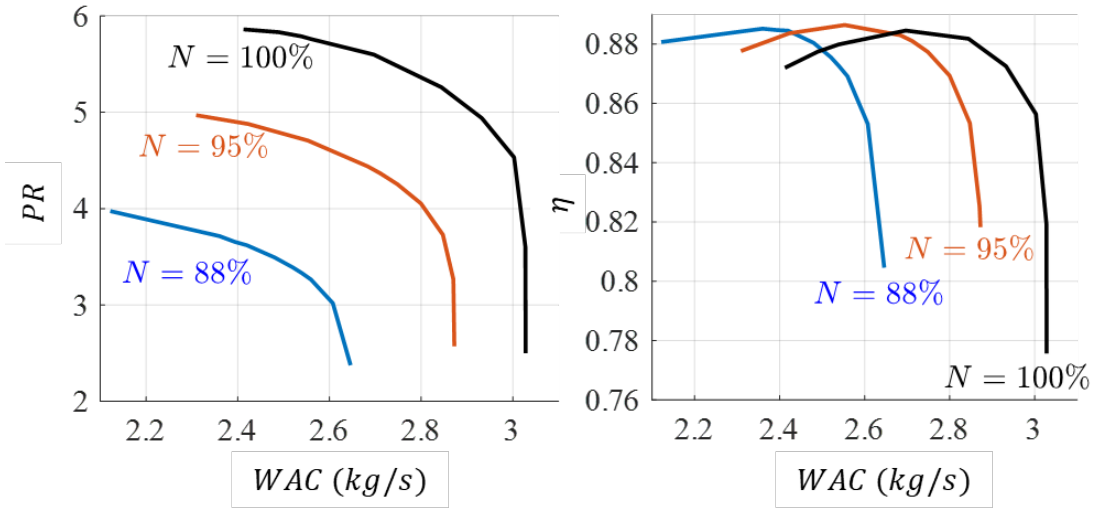

Fig. 2. Compressor operating map [27]

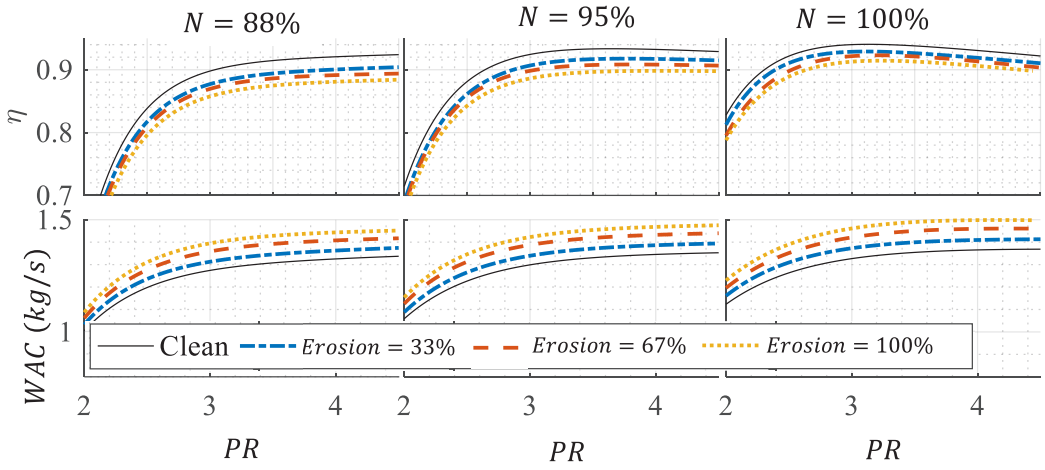

Fig. 3. Turbine operating map [29]

$$PR_t = \frac{P_{o3}}{P_{o4}} \tag{12}$$

As mentioned previously, in this research, the operating characteristic curves of a radial turbine from Ref. [29] are used. The curves are shown **Fig. 3**.

3- 3- Combustion chamber operation

In order to model combustion chamber performance, combustion efficiency, and pressure loss are considered to be two critical parameters. The main factor contributing to pressure loss in the combustion chamber is wall friction, and other factors are negligible [32]. So, the pressure loss of the combustion chamber in the operating range can be approximated by Eq. 13 [45].

$$\Delta P_o = P_o \cdot \left(\frac{\Delta P_o}{P_o}\right)_D \cdot \left[\left(\dot{m}\sqrt{T_o}/P_o\right)/\left(\dot{m}\sqrt{T_o}/P_o\right)_D\right]^2 \tag{13}$$

Where ΔP is the pressure drop. For the design condition, the pressure drop is assumed to be 2% of the inlet pressure [46]. The mass flow is given in **Table 1**. Combustion efficiency variation can be ignored within the operating range of the engine [32]. So in this research, it is assumed to be fixed.

3- 4- Recuperator Operation

The recuperator performance parameters are pressure loss and effectiveness. The values of these parameters are related to operating conditions as below:

3- 4- 1- Effectiveness

Eq. (14) presents the off-design behavior of recuperator effectiveness [45]. The design value of the effectiveness is 90%.

$$\varepsilon = 1 - \frac{\dot{m}}{\dot{m}_D} \cdot \left(1 - \varepsilon_D\right) \tag{14}$$

3- 4- 2- Pressure Loss

The pressure drop of the recuperator has the same nature as burner friction loss. So Eq. (13) can be used here too for both the cold side (between the compressor and combustion chamber) and hot side (between the turbine and the exhaust) of the recuperator.

3- 5- Generator Operation

Part load power of a variable high-speed generator can be calculated through Eq. 15.[33, 47].

In which W is power. Design condition values of power and shaft speed are given in **Table 1**.

$$W_{gen} = W_D \cdot \left(\frac{N}{N_D}\right)^{3.97} \tag{15}$$

3- 6- Compatibility Equations

Recognizing, that the turbine's produced power is totally absorbed by the compressor and generator compressor, power compatibility should be satisfied as equation Eq. 16.

$$W_t = \frac{W_c}{\eta_m} + \frac{W_{gen}}{\eta_m} \tag{16}$$

The turbine mass flow is supplied by the compressor crossed flow so mass flow conservation (Eq. (17)) and pressure distribution compatibility equation (Eq. (18)) should be satisfied too.

$$\dot{m}_g = \dot{m}_a + \dot{m}_f \tag{17}$$

$$PR_t = PR_c \cdot \left(1 - \frac{\Delta P_o^{c.c}}{P_{o5}}\right) \cdot \left(1 - \frac{\Delta P_{o,rcs}}{P_{o2}}\right) \cdot \left(1 - \frac{\Delta P_{o,rhs}}{P_{o4}}\right) \tag{18}$$

Moreover, the turbine and the compressor are located in the same shaft so the rotational speed of the turbine and compressor should be equal which can be stated as the rotational speed compatibility equation (Eq. 19).

$$N_{cor,t} = N_{cor,c} \cdot \sqrt{\frac{T_{o1}}{T_{o3}}} \tag{19}$$

3- 7- Micro Turbine off-design performance system of equations

All the equations presented in the above sections are listed in **Table 2**. As shown in this table, the off-design operation of MGT, can be mathematically simulated by solving a combination of nine characteristic equations of the components and four compatibility equations that construct a system of nonlinear equations. These total thirteen equations comprise fourteen unknowns. As the value of demand power is determined, the governing system of equations is confined and can be solved.

4- Result and Discussion

In the current section, at first, validation of the proposed model of the MGT is presented, and then erosion test cases are described. To validate the off-design model, the operating data of Turbec 100 MGT is used. In the following, the MGT running line, under the clean and eroded turbine blade condition, is determined and reported in the form of parameters relative variation. At last, results are evaluated to select the best parameters for detecting turbine blade erosion.

4- 1- Validation

Running line data of Turbec 100 MGT is accessible in several articles such as Refs [37, 48-50]. For example, in Ref. [50] the test rig was based on a commercial Turbec 100 MGT installed. In the mentioned research, in addition to standard instrumentation, the test rig was equipped with additional sensors to allow monitoring and analysis of additional performance parameters. The sensors made it possible to measure pressure and temperature in the compressor inlet and outlet and combustion chamber inlet. Furthermore, a high-temperature thermocouple positioned in the combustor can exit was used to measure the combustor outlet temperature [50]. The mentioned test rig is shown in **Fig. 4**.

The data of the mentioned Refs are used to validate the off-design simulation of the current study. The design point technical data are given in **Table 1**. It should be mentioned that Turbec 100 is fueled by natural gas, and for this modeling, ambient air is at $20°C$ and $100\ kPa$. The result of Turbec 100 MGT simulation by the current research method and experimental data from [48] are compared in **Fig. 5**. In this figure, the error percent is illustrated on the right axis of each graph. As it can be seen, the prediction of the proposed model shows appropriate fitness with the experiment data so that all errors are below 1.8%.

4- 2- Erosion Test Case

In order to study the effects of turbine erosion on the performance of the MGT, the operating maps of a radial turbine from Ref. [29] are applied. In the mentioned research,

Table 2. List of equations that govern off-design operation of MGT

	Equation name	variables	New Unknown
Components Characteristics Equations	Compressor mass Flow	1) $f_1(X_1, X_2, X_3) = 0$ (From Fig. 2)	1. $X_1 = \mathrm{WAC_c}$ 2. $X_2 = \mathrm{PR_c}$ 3. $X_3 = N_{cor,c}$
	Compressor Efficiency	2) $f_2(X_1, X_2, X_4) = 0$ (From Fig. 2)	4. $X_4 = \eta_c$
	Turbine Mass flow	3) $f_3(X_5, X_6, X_7) = 0$ (From Fig. 3)	5. $X_5 = WAC_t$ 6. $X_6 = PR_t$ 7. $X_7 = N_{cor,t}$
	Turbine Efficiency	4) $f_4(X_6, X_7, X_8) = 0$ (From Fig. 3)	8. $X_8 = \eta_t$
	Recuperator Effectiveness	5) $f_1(X_1, X_2, X_3, X_9) = 0$ (From Eq. 14)	9. $X_9 = \varepsilon$
	Recuperator cold side Pressure Loss	6) $f_6(X_{10}) = 0$ (Extracted from Eq. 13)	10. $X_{10} = \Delta P_{o,rcs}$
	Combustion Chamber Pressure Loss	7) $f_7(X_{11}) = 0$ (Extracted from Eq. 13)	11 $X_{11} = \Delta P_{o,CC}$
	Recuperator hot side Pressure Loss	8) $f_8(X_{12}) = 0$ (Extracted from Eq. 13)	12. $X_{12} = \Delta P_{o,rhs}$
	Generator	9) $f_9(X_4, X_{13}) = 0$ (From Eq. 15)	13. $X_{13} = Power$
Compatibility Equations	Rotational speed	10) $f_4(X_3, X_7, X_{14}) = 0$ (From Eq. 19)	14. $X_{14} = \frac{T_{o3}}{T_{o1}}$
	Pressure Distribution	11) $f_{11}(X_2, X_6, X_{10}, X_{11}, X_{12}) = 0$ (From Eq. 18)	
	Mass flow	$f_{12}(X_1, X_2, X_5, X_{14}) = 0$ (From Eq. 17)	
	Power	13) $f_{13}(X_1, X_2, X_4, X_5, X_6, X_8, X_{13}, X_{14}) = 0$ (From Eq. 16)	

three levels of turbine blade erosion were considered: 33%, 67%, and 100 erosion intensities. The effects of these erosion levels were simulated through three-dimensional CFD modeling, and turbine operating maps were achieved. The operating maps are shown in **Fig. 3** which demonstrate that the turbine expansion ratio does not experience significant change. However, isentropic efficiency falls, and corrected mass flow increases considerably when the blade erodes.

4- 3- Performance deterioration in partial load

The MGT behavior in three different severities of turbine erosion is investigated. To do this, performance parameters for three partial loads (60.2%, 81.6%, and 100% of the maximum load) are computed. Eroded performance parameters deviations from the clean condition are presented in **Fig. 6**, **Fig. 7**, and **Fig. 8**. The Changes in fuel mass flow, thermal efficiency, and turbine inlet temperature are shown in these figures respectively. By investigation of these figures, it can be understood that the parameters' deviations are intensified by erosion increase. In the case of fuel mass flow and thermal efficiency, deviations rise with load increment; however, TIT deviation reduces with load increment. The overall conclusion would be that the fuel mass flow and turbine inlet temperature rise while thermal efficiency falls. As it is expected, all these changes are in the direction of performance dropping. The deviation of the compressor pressure ratio and the air mass flow are shown in **Fig. 9**. Air mass flow rises, but the relative deviation reduces with load increment. As is shown, turbine erosion leads to an increment in turbine mass flow at each rotational speed by a similar pressure ratio, so it moves the running point to higher air mass flow. Higher air mass flow in the compressor map necessitates a lower pressure ratio,

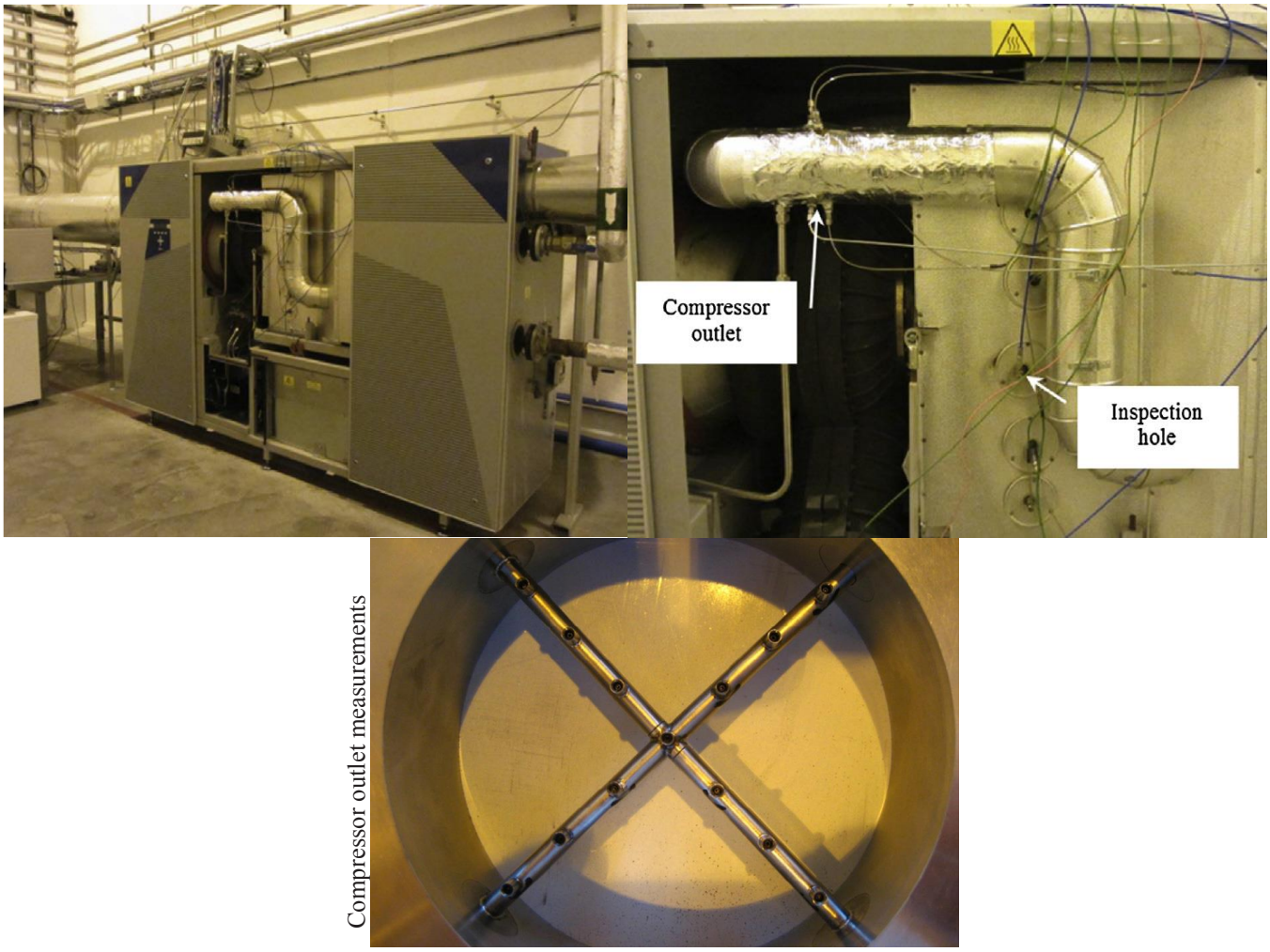

Fig. 4. Turbec 100 MGT test Rig [49, 50]

so the compressor pressure ratio decreases as the erosion rises. Therefore, it can be said that the increase in fuel flow is caused by three factors. Firstly, the increase in the air mass flow rate of the compressor is a direct result of increasing the flow rate of the turbine due to erosion. Secondly, the increase in the inlet temperature of the turbine is caused by the decrease in turbine efficiency due to erosion and the decrease in the efficiency of the compressor operating point due to going out of the design conditions. Third, the reduction of the compressor discharge temperature occurs due to moving the compressor operating point to areas with lower pressure ratios. As mentioned previously in section (3-5), load fraction is directly correlated with shaft rotational speed. So the shape of the compressor characteristic in each rotational speed determines the quantity of pressure ratio variation against mass flow rise in that rotational speed and correlatively in that load fraction. Variations of the compressor pressure ratio and air mass flow relative deviations with load fraction originated by this content. The coupling of all MGT components imposes this variation to spread and appears in the behavior of other components and performance parameters.

4- 4- Performance parameters response to turbine erosion

Knowing the MGT response to component damage helps the operator take appropriate actions to fix the problem. To analyze the engine response deviation of several gas paths and performance parameters are shown in **Fig. 10**. The parameters are compressor pressure ratio (*PR*), specific fuel consumption (*SFC*), thermal efficiency (η_{th}), fuel mass flow rate ($\dot{m}_f$), air mass flow rate ($\dot{m}_a$), compressor discharge temperature (T_{o2}), combustion chamber inlet temperature (T_{o5}), Turbine Inlet Temperature ($TIT \sim T_{o3}$),

turbine exhaust temperature ($TET \sim T_{o4}$), recuperator hot exhaust temperature (T_{o6}), and recuperator effectiveness (ε). In this figure, only the maximum intensity of erosion (Erosion Intensity=100%) is examined, and three columns are presented for each parameter, each column is representative of deviation in a special engine load fraction. This figure reveals that T_{o3},

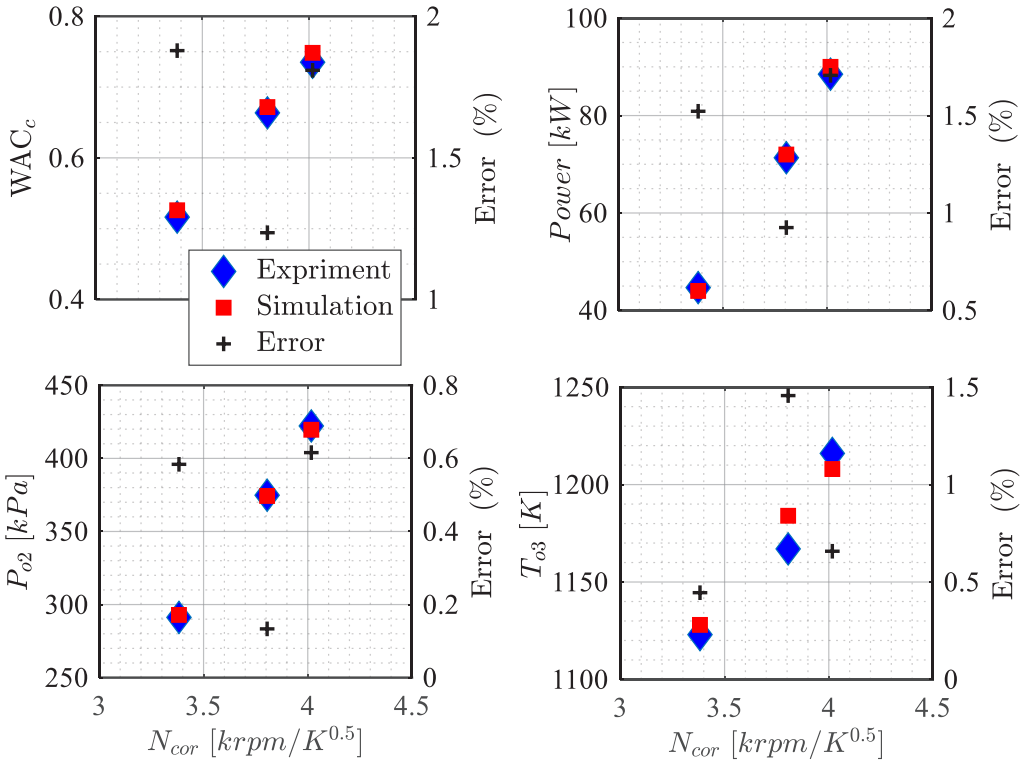

Fig. 5. Comparison of proposed model predictions and experimental data of Turbec 100 running line

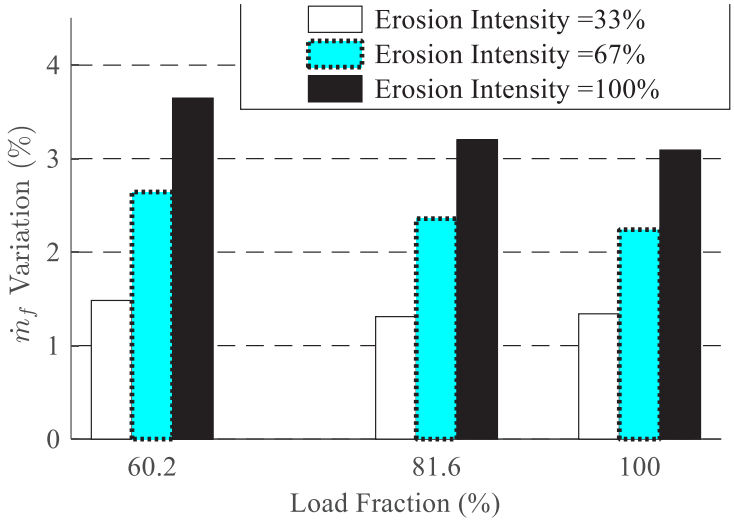

Fig. 6. Variation of fuel mass flow in different Loads and Erosion levels

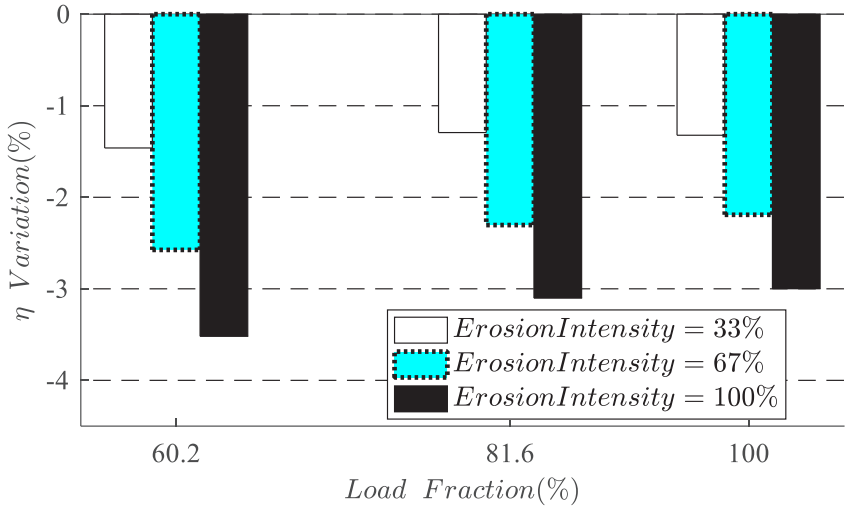

Fig. 7. Variation of Thermal efficiency in different Loads and Erosion levels

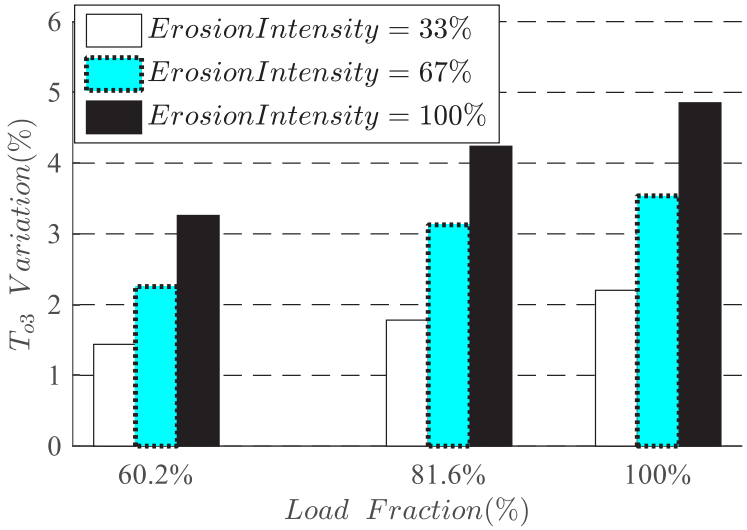

Fig. 8. Variation of TIT in different Loads and Erosion levels

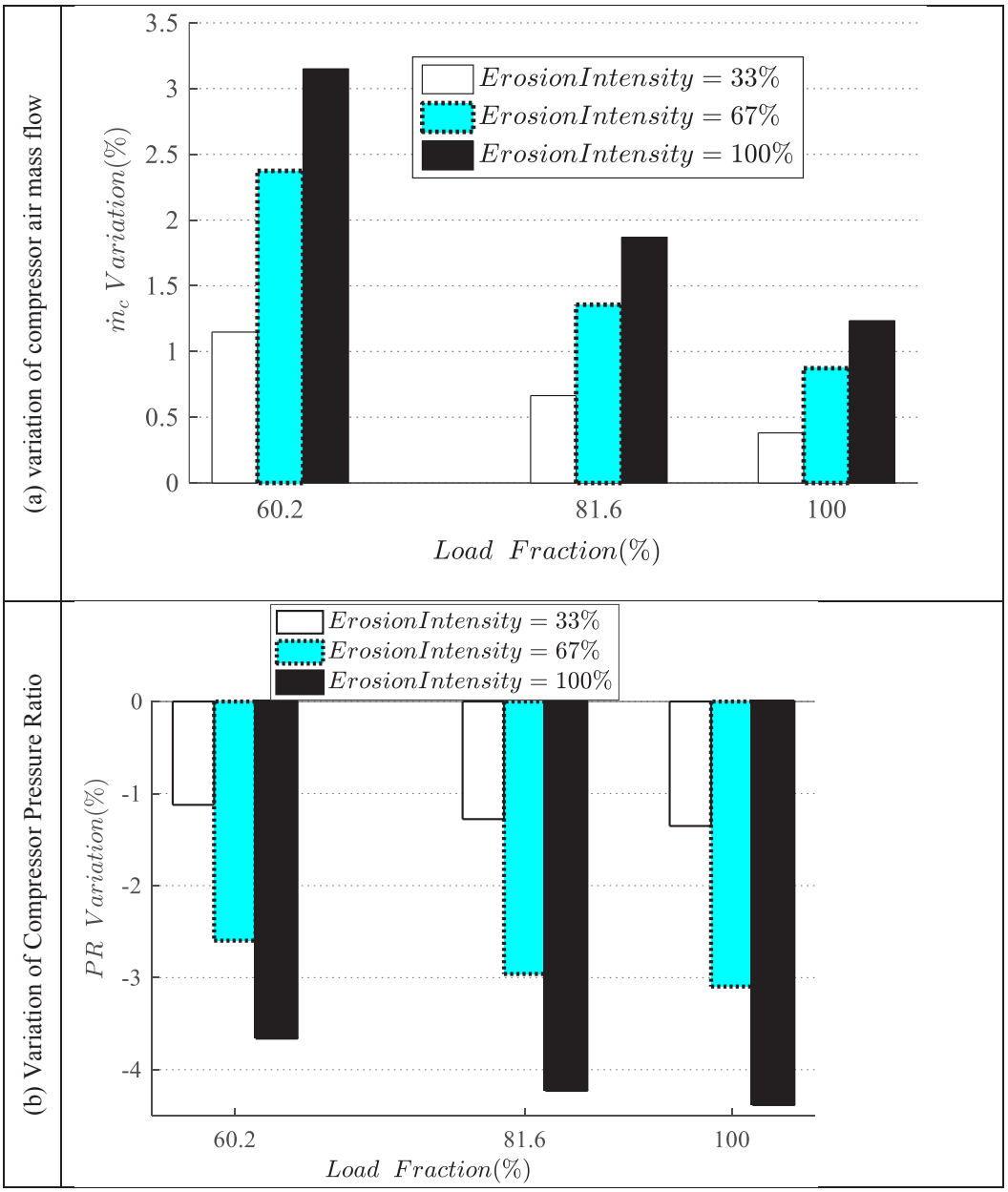

Fig. 9. Variation of Air mass flow (a) and compressor pressure ratio (b) in different Loads and Erosion levels

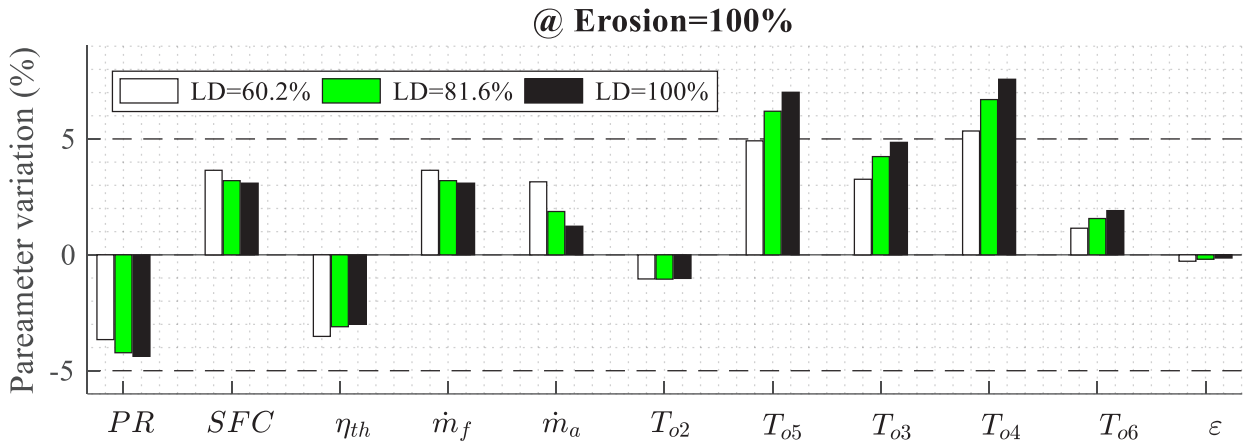

Fig. 10. Effects of load change on the gas path and performance parameters in Maximum Erosion level

T_{o4} and T_{o5} rise dramatically in the effect of turbine erosion while $\dot{m}_a$, T_{o2} and T_{o6} experience small changes. As can be seen in **Fig. 10**, compressor *PR* experiences a considerable drop, and consequently, a significant decrease in T_{o2} is expected, but what has happened is a small change of T_{o2}. To analyze this behavior, another effective parameter should be considered. When the turbine erosion moves the engine running point to a lower pressure ratio area, compressor isentropic efficiency falls simultaneously. According to Eq. (1), while pressure ratio reduction makes the required work of the compressor lower, isentropic efficiency drop makes it higher. So these two phenomena neutralize each other, and consequently, *CDT* does not experience considerable variation. Another notable event is the variation of T_{o3}, T_{o5}, and T_{o4}. The turbine's erosion increases losses and reduces its power output. On one hand, to compensate for this loss, turbine inlet temperature (T_{o3}) rises, and on the other hand, turbine erosion moves the running point to a lower pressure ratio. Both of these two changes move the turbine outlet temperature (T_{o4}) to a higher value, so T_{o4} experiences a higher rise than T_{o3}. According to Eq. (2). T_{o5} is a function of T_{o2}, T_{o4}, and recuperator effectiveness (ε). As it is cleared in **Fig. 10**, both T_{o2} and ε experience a small reduction, while T_{o4}, as discussed, rises dramatically. So the superimposition of these changes leads to a considerable rise in T_{o5}. To summarize the sensitivity analysis of different parameters of MGT, it can be concluded that T_{o4}, T_{o5}, and compressor *PR* as measurable parameters, show the most sensitivity to turbine erosion. A small Reduction in T_{o2} simultaneous with some increases in other sections' temperature should be considered as evidence of turbine erosion.

4- 5- Investigation of Operating Line status

As it is shown previously in Fig. 3 the blade erosion changes the turbine characteristic curves, which leads to a shift in the running line. In Fig. 11 the location of MGT running line is shown in the compressor characteristics. Here the control scenario is maintaining the output power and the second is maintaining the TIT. In Fig. 11-a location of the running line in the compressor PR-mass flow characteristic is shown, while the control scenario maintains the output power. We can see Fig. 11-a, that when the turbine is eroded, the running line shifts to a new location with a higher $\dot{m}_a$ and a lower PR. Moreover, TIT rises significantly. In this condition, the surge margin is increased too. The location of the running lines under the turbine normal and eroded conditions in the compressor efficiency-mass flow characteristic are illustrated in Fig. 11-b, the control scenario is still maintaining the output power. This figure reveals that the running line is moved to lower the isentropic efficiency of the compressor.

In the turbine map, η_s falls due to the erosion losses (see Fig. 3) and PR reduces in the effect of coupling with compressor operation change. An increase in $\dot{m}_a$ induces a lower required specific power, which consequently reduces the required *TIT*. However, at the same time, the drop η_s in the compressor (**Fig. 11**- b) and turbine results in a reduction of available specific power. The current effect necessitates *TIT* increase to compensate η_s for drop losses. Altogether, the effect of the later parameter is predominant, and *TIT* increases due to turbine erosion. Another matter that should be discussed is the variation of recuperator and combustion chamber pressure loss. The variation of the pressure loss in these components is shown in **Fig. 12**. To interpret **Fig. 12** we can refer to Eq. 13, which shows the pressure loss of the recuperator and the

combustion chamber is directly proportional to the inlet mass flow and total temperature and inversely proportional to the inlet total pressure. Moreover, as shown in **Fig. 10**, due to the turbine erosion, $\dot{m}_a$ increases and *PR* decreases, which means the recuperator cold side inlet pressure reduces and

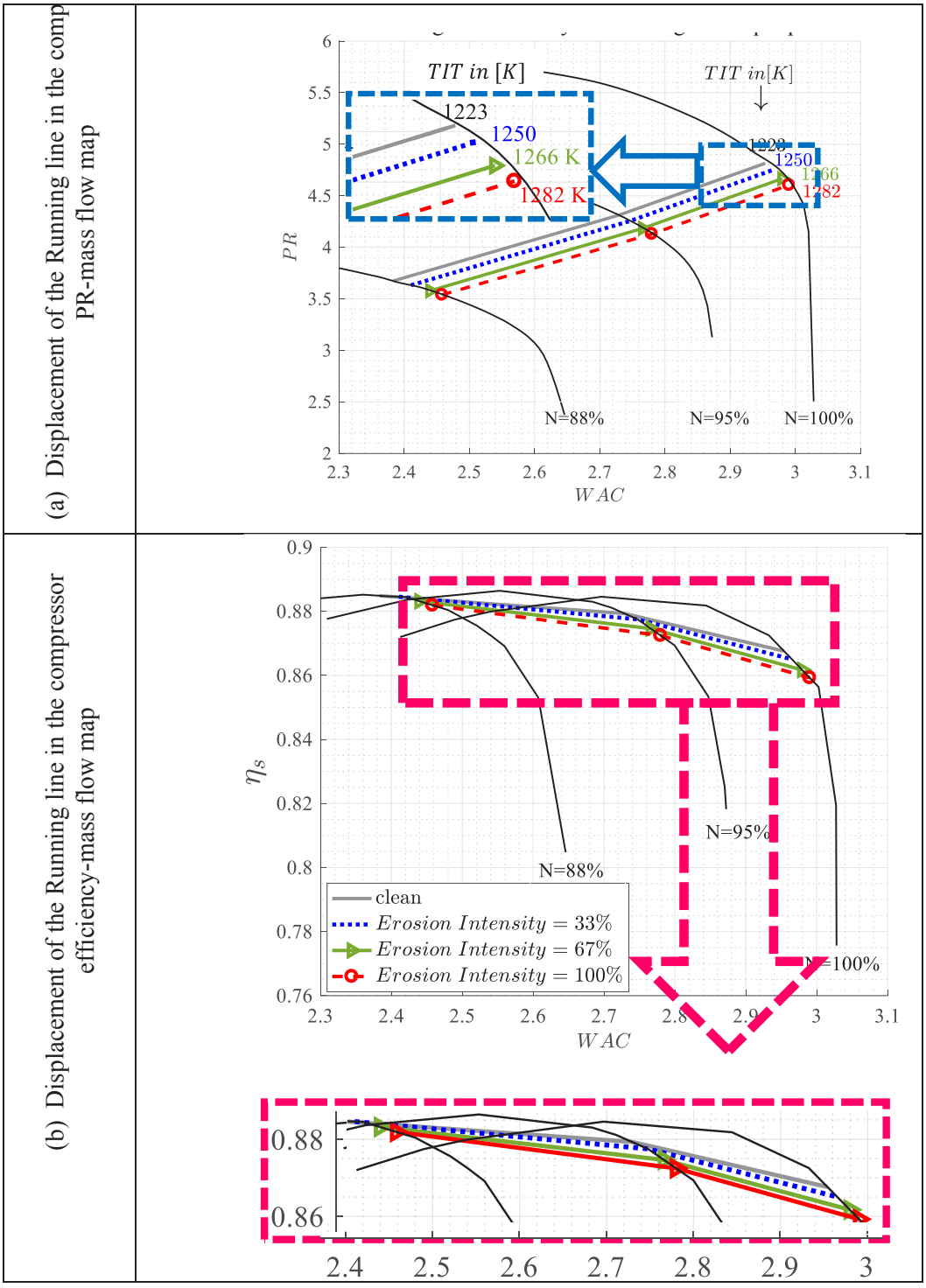

Fig. 11. Displacement of the Running line in the compressor map by maintaining the output power

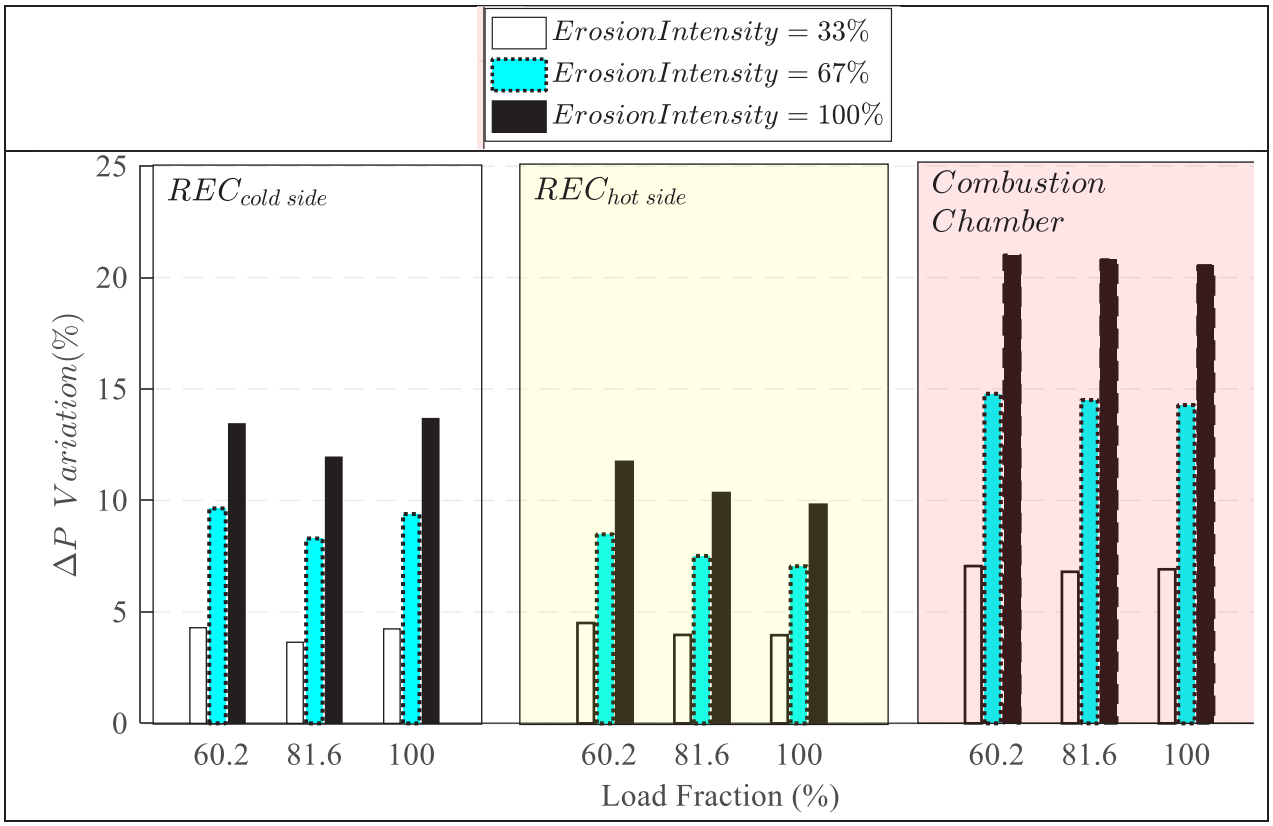

Fig. 12. Change of pressure losses in burner and recuperator against load and erosion level

the recuperator inlet temperature decreases slightly. Effects of $\dot{m}_a$ and pressure changes dominate the temperature effect, and pressure loss on the recuperator's cold side increases. Referring to Eq. 13 and **Fig. 10** helps to compare the pressure loss of the combustion chamber in clean and eroded conditions. When airflow exits the recuperator, two factors have intensified conditions toward the reduction of the combustion chamber pressure. The first is the reduction of PR, and the other is the increased pressure loss of the recuperator. On the other hand, both inlet mass flow and temperature in the combustion chamber are increased (as shown in **Fig. 10**), so the variations of all these three parameters induce a higher pressure loss in the combustion chamber. So the pressure drop change in the combustion chamber experiences a higher value with respect to the recuperator cold side in the eroded state. The status on the recuperator hot side has some small differences. As shown in **Fig. 10**; in the eroded condition, airflow, inlet temperature (T_{o4}), and pressure (P_{o4}) of the recuperator hot side increase. While the two first changes intend to increase pressure loss, the latter one acts inversely and decreases pressure loss, so the pressure loss of the recuperator hot side experiences a lower increase. As mentioned previously, turbine erosion reduces turbine isentropic efficiency (η_s). In the new conditions, due to the running line shift in the compressor map, the compressor isentropic efficiency (η_c) falls too. Moreover, as discussed above, pressure losses (in the recuperator and combustion chamber) grow, so the latter event should be considered as another reason that has intensified the *TIT* rise too.

4- 6- Engine behavior in an acceptable temperature area

As discussed in previous sections, due to the turbine erosion in MGT, not only performance parameters such as η_{th} fall down but also *TIT* grows up. Since higher temperatures damage the turbine blade, intensify its degradation rate, and consequently reduce its remained operating life, regardless of other parameters, the rise in *TIT* is an undesirable event that should be avoided. Limiting turbine inlet temperature results in

a new running condition, which should be analyzed separately to estimate eroded turbine operating costs and achieve more effective health condition monitoring. Moreover, if maintaining the maximum *TIT* is applied as the control constraint, the pattern of the parameter's variation may differ. To take into account the effect of this constraint and present a comparison between these two control scenarios. Variation patterns of the engine parameters are presented in the first row of **Fig. 13 (a to c)** for maintaining the maximum output

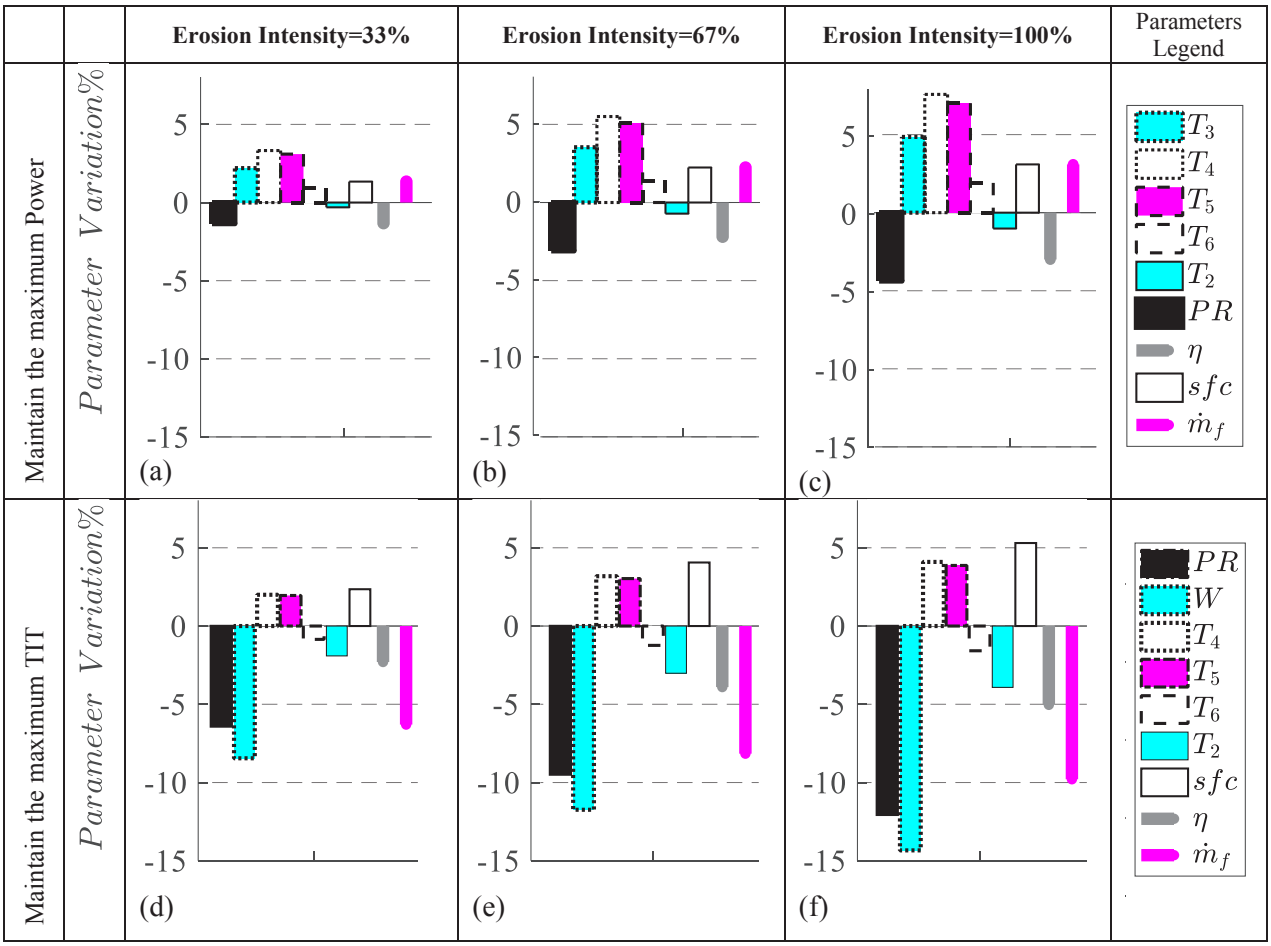

Fig. 13. Change of gas path and performance parameters by Erosion intensity rise by maintaining the maximum output power and maintaining the maximum temperature limit

power scenario and in the second row of **Fig. 13 (d** to **f)** for maintaining the maximum *TIT* scenario. For each scenario, variations are illustrated for Erosion Intensity =33%, 67%, and 100 in column 1, column 2, and column 3 respectively. According to **Fig. 13-a** to **c**. by maintaining the maximum output power, *CDT* (T_{o2}) decreases slightly, and RET (T_{o6}) experiences a few increases. Fuel mass flow rate ($\dot{m}_f$) and *SFC* rise by the same values and η_{th} experience the same value change but in the reverse direction. Altogether, it can be seen that T_{o2}, T_{o6}, $\dot{m}_f$, SFC, and thermal efficiency are not very sensitive to turbine erosion while

the pressure ratio, T_{o5}, $T_{o3,}$ and specifically $T_{o4,}$ are very sensitive. T_{o4} shows the most intense reaction to turbine erosion when the output power is fixed. According to **Fig. 13**-d to f in the maximum allowable *TIT* control scenario, parameter variations show different behavior compared with the previous state. With this new constraint, *PR*, and power (*W*) reduced dramatically. Moreover, $\dot{m}_f$ decreased intensively while, in the previous case, experienced a few rises. T_{o6} already increased slightly and now shows a few reductions. However, T_{o3} remains fixed, but due to the reduction of *PR*, T_{o4} rises. A higher T_{o4} increases T_{o5} by increasing the heat transfer in the recuperator. As it is obvious in **Fig. 13-**d to f, by maintaining the maximum *TIT*, new parameters show higher sensitivities compared with the other scenario. So when *TIT* is maintained, net power (*W*), *PR*, and $\dot{m}_f$ are the most sensitive parameters to turbine erosion. Previously, in **Fig. 11** running line shift due to erosion was shown while output power was maintained. If we apply maintaining the maximum *TIT* limitation as a constraint **Fig. 14** would be resulted. This figure shows, how maintaining the maximum *TIT* will result in a drop in the output power. Since *TIT* in each rotational speed raises due to erosion, to maintain maximum *TIT*, rotational speed will be limited. As

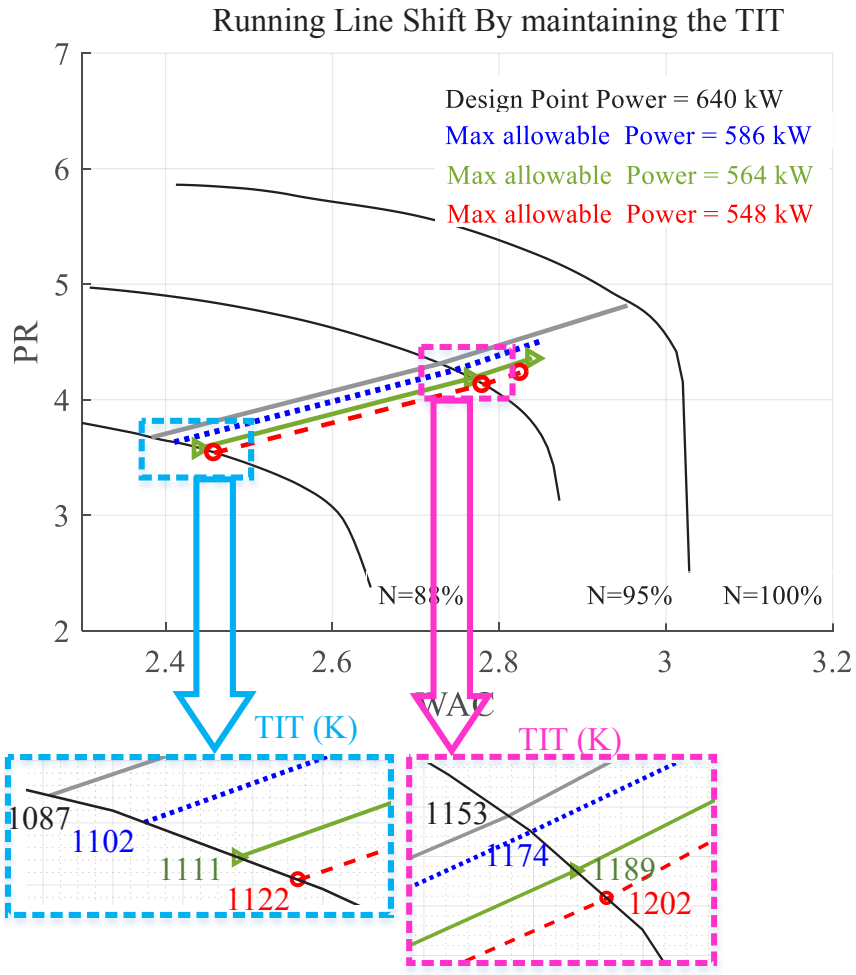

Fig. 14. Displacement of the Running line in the compressor map by maintaining the maximum TIT

expressed in Eq. 15 the generator power is directly a function of rotational speed. So a reduction in rotational speed leads to a drop in the generator power, which is shown in **Fig. 13** too.

5- Conclusion

In this study, the reaction of a MGT to turbine blade erosion in both full and part load operation is investigated. It has been understood that the performance parameters deviation in the effect of erosion is intensified by erosion severity. The variation of parameters is also a function of the power fraction of MGT.

Also, the most sensitive and insensitive parameters to turbine erosion with and without *TIT* limitation has been determined. The analysis reveals that without *TIT* limitation, compressor pressure ratio, combustion chamber inlet temperature, and specifically turbine outlet temperature are the most sensitive parameters and the best parameters to sense turbine erosion while compressor discharge temperature and recuperator exhaust temperature are approximately affectless parameters. Moreover, with *TIT* limitation, fuel mass flow, PR, and specifically generator power show significant changes, but compressor discharge temperature and recuperator exhaust temperature are still affectless parameters.

These results aid in tuning the fault detection system and help have better health condition monitoring by a minimum number of detector sensors and earlier detection to prevent damage growth. An effective fault detection system may lead to reduce the number of required visual inspections and consequently, MGT breaking down, which decreases maintenance and operation costs.

The blade erosion effects on the steady-state behavior of a MGT are investigated in this research. Foster analysis about MGT steady and transient behavior when both compressor fouling and turbine erosion happen at the same time can be useful.

Nomenclature

CDT	Compressor Discharge Temperature, K
CL	Clean
Cp	Heat Capacity, kJ/kg/K
LHV	Lower Heating Value, kJ/kg
$\dot{m}$	Mass flow rate, kg/s
N	Rotational Speed, RPM
P	Pressure, kPa
PR	Pressure Ratio
SFC	Specific fuel consumption, kg/kW/hr
T	Temperature, K
TET	Turbine Exhaust Temperature, K
TIT	Turbine inlet Temperature, K
w	Power, kW
WAC	Corrected Mass flow rate, kg/s

Greek Symbols

γ	Heat Capacity Ratio
ε	Effectiveness
η	Efficiency

Subscript

a	Air
c	Compressor
CC	Combustion Chamber
cor	corrected
D	Design
f	fuel
g	Hot gas
gen	generator
o	Zero condition
rcs	Recuperator cold side
rhs	Recuperator hot side
s	Standard condition
t	Turbine
th	thermal

References

[1] M. Badami, P. Nuccio, A. Signoretto, Experimental and numerical analysis of a small-scale turbojet engine, Energy Conversion and Management, 76(0) (2013) 225-233.

[2] A. Gimelli, R. Sannino, A multi-variable multi-objective methodology for experimental data and thermodynamic analysis validation: An application to micro gas turbines, Applied Thermal Engineering, 134 (2018) 501-512.

[3] M. Javidmehr, F. Joda, A. Mohammadi, Thermodynamic and economic analyses and optimization of a multi-generation system composed by a compressed air storage, solar dish collector, micro gas turbine, organic Rankine cycle, and desalination system, Energy Conversion and Management, 168 (2018) 467-481.

[4] C.M. Bartolini, F. Caresana, G. Comodi, L. Pelagalli, M. Renzi, S. Vagni, Application of artificial neural networks to micro gas turbines, Energy Conversion and Management, 52(1) (2011) 781-788.

[5] M. Mirzaee, R. Zare, M. Sadeghzadeh, H. Maddah, M.H. Ahmadi, E. Acıkkalp, L. Chen, Thermodynamic analyses of different scenarios in a CCHP system with micro turbine – Absorption chiller, and heat exchanger, Energy Conversion and Management, 198 (2019) 111919.

[6] S. Talebi, A. Tousi, The effects of compressor blade roughness on the steady state performance of micro-turbines, Applied Thermal Engineering, 115 (2017) 517-527.

[7] S. Mazzoni, G. Cerri, L. Chennaoui, A simulation tool for concentrated solar power based on micro gas turbine engines, Energy Conversion and Management, 174 (2018) 844-854.

[8] B. Dehghan B, Performance assessment of ground source heat pump system integrated with micro gas turbine: Waste heat recovery, Energy Conversion and Management, 152 (2017) 328-341.

[9] Micro Gas Turbine Technology Summary, ETN Global, 2016.

[10] N. Aldi, N. Casari, M. Morini, M. Pinelli, P.R. Spina, A. Suman, Gas Turbine Fouling: A Comparison Among 100 Heavy-Duty Frames, Journal of Engineering for Gas Turbines and Power, 141(3) (2018) 032401-032401-032412.

[11] E. Mohammadi, M. Montazeri-Gh, Simulation of Full

and Part-Load Performance Deterioration of Industrial Two-Shaft Gas Turbine, Journal of Engineering for Gas Turbines and Power, 136(9) (2014) 092602-092609.

[12] M.J. Kim, J.H. Kim, T.S. Kim, The effects of internal leakage on the performance of a micro gas turbine, Applied Energy, 212 (2018) 175-184.

[13] E. Mohammadi, M. Montazeri-Gh, Performance enhancement of global optimization-based gas turbine fault diagnosis systems, Journal of Propulsion and Power, 32(1) (2015) 214-224.

[14] M. Tahan, E. Tsoutsanis, M. Muhammad, Z.A. Karim, Performance-based health monitoring, diagnostics and prognostics for condition-based maintenance of gas turbines: A review, Applied energy, 198 (2017) 122-144.

[15] A.A. Hamed, W. Tabakoff, R. Wenglarz, Erosion, Deposition, and Their Effect on Performance, in: Turbine Aerodynamics, Heat Transfer, Materials, and Mechanics, American Institute of Aeronautics and Astronautics, Inc., 2014, pp. 585-611.

[16] T.S. Kim, Model-based performance diagnostics of heavy-duty gas turbines using compressor map adaptation, Applied Energy, 212 (2018) 1345-1359.

[17] A. Kellersmann, S. Weiler, C. Bode, J. Friedrichs, J. Städing, G. Ramm, Surface Roughness Impact on Low-Pressure Turbine Performance Due to Operational Deterioration, Journal of Engineering for Gas Turbines and Power, 140(6) (2018) 062601-062601-062607.

[18] E. Tsoutsanis, N. Meskin, Derivative-driven window-based regression method for gas turbine performance prognostics, Energy, 128 (2017) 302-311.

[19] S.S. Talebi, A. Madadi, A.M. Tousi, M. Kiaee, Micro Gas Turbine fault detection and isolation with a combination of Artificial Neural Network and off-design performance analysis, Engineering Applications of Artificial Intelligence, 113 (2022) 104900.

[20] M. Badami, M.G. Ferrero, A. Portoraro, Dynamic parsimonious model and experimental validation of a gas microturbine at part-load conditions, Applied Thermal Engineering, 75 (2015) 14-23.

[21] Y. Qingcai, S. Li, Y. Cao, N. Zhao, Full and Part-Load Performance Deterioration Analysis of Industrial Three-Shaft Gas Turbine Based on Genetic Algorithm, in: ASME Turbo Expo 2016: Turbomachinery Technical Conference and Exposition, American Society of Mechanical Engineers, 2016, pp. V006T005A016-V006T005A016.

[22] D. Amare, T. Aklilu, S. Gilani, Effects of performance deterioration on gas path measurements in an industrial gas turbine, ARPN J. of Engineering, 11 (2016) 14202-14207.

[23] D. Zhou, T. Wei, D. Huang, Y. Li, H. Zhang, A gas path fault diagnostic model of gas turbines based on changes of blade profiles, Engineering Failure Analysis, 109 (2020) 104377.

[24] M. Montazeri-Gh, A. Nekoonam, Gas path component fault diagnosis of an industrial gas turbine under different load condition using online sequential extreme learning machine, Engineering Failure Analysis, 135 (2022) 106115.

[25] K. Brun, M. Nored, and R. Kurz, Analysis of Solid Particle Surface Impact Behavior in Turbomachines to Assess Blade Erosion and Fouling, in: Forty-First Turbomachinery Symposium, Houston, Texas: Turbomachinery Laboratory, Texas A&M University, 2012.

[26] P. Bauwens, Gas path analysis for the MTT micro turbine, Delft University of technology, 2015.

[27] S.S. Talebi, A. Mesgarpoor Tousi, Investigation of Compressor Blade Roughness Increment Effect on Micro Turbine Performance, Amirkabir Journal of Mechanical Engineering, 49(3) (2017) 471-484.

[28] S. Talebi, A. Tousi, A. Madadi, M. Kiaee, A methodology for identifying the most suitable measurements for engine level and component level gas path diagnostics of a micro gas turbine, 236(5) (2022) 2646-2661.

[29] M. Pourhasan, Effect of component degradation on gas turbine performance, Amirkabir University of Technology, 2018.

[30] M. Kiaee, A.M. Tousi, Vector-Based Deterioration Index for Gas Turbine Gas-Path Prognostics Modeling Framework, Energy, (2020) 119198.

[31] P. Pilavachi, Power generation with gas turbine systems and combined heat and power, Applied Thermal Engineering, 20(15) (2000) 1421-1429.

[32] H. Cohen, G. Rogers, H. Saravanamuttoo, Gas turbine theory, 1996, London, UK.

[33] M. Kiaee, A. Tousi, M. Toudefallah, Performance adaptation of a 100 kW microturbine, Applied Thermal Engineering, 87 (2015) 234-250.

[34] K. Thu, B.B. Saha, K.J. Chua, T.D. Bui, Thermodynamic analysis on the part-load performance of a microturbine system for micro/mini-CHP applications, Applied Energy, 178 (2016) 600-608.

[35] W. Wang, R. Cai, N. Zhang, General characteristics of single shaft microturbine set at variable speed operation and its optimization, Applied Thermal Engineering, 24(13) (2004) 1851-1863.

[36] T100 Detailed Specifications, in, Turbec, 2009.

[37] M.M. Majoumerd, H.N. Somehsaraei, M. Assadi, P. Breuhaus, Micro gas turbine configurations with carbon capture - Performance assessment using a validated thermodynamic model, Applied Thermal Engineering, Volume 73(1) (2014) 172-184.

[38] H. Saito, Micro gas turbine risks and market in: International Association of Engineering Insurers (IMIA), Stokholm, Sweden, 2003.

[39] P. Akbari, R. Nalim, N. Müller, Performance Enhancement of Microturbine Engines Topped With

Wave Rotors, Journal of engineering for gas turbines and power, 128(1) (2006) 190-202.

[40] M.A.R. Nascimento, L. Rodrigues, E. Santos, E.E.B. Gomes, F.L.G. Dias, E.I.G. Velásques, R.A.M. Carrillo, Micro gas turbine engine: a review, in: E. Benini (Ed.) Progress in gas turbine performance, InTech, Rijeka, Croatia, 2014, pp. 107-141.

[41] P1012 C600 600kW Power Package HP Natural Gas Capstone Turbine Corporation, 2010.

[42] 100 kW CHP Microturbine, in, Elliott Microturbines, 2005.

[43] F. Bozza, A. Pontecorvo, F. Reale, R. Tuccillo, Analisi Del Funzionamento A Regime Ed In Transitorio Di Una Microturbina A Gas, in: 60° Congresso Nazionale ATI, Roma, 2005.

[44] C. Wei, S. Zang, Experimental Investigation on the Off-Design Performance of a Small-Sized Humid Air Turbine Cycle, Applied Thermal Engineering, 51 (2013).

[45] P.P. Walsh, P. Fletcher, Gas turbine performance, John Wiley & Sons, 2004.

[46] D.P. Bakalis, A.G. Stamatis, Full and part load exergetic analysis of a hybrid micro gas turbine fuel cell system based on existing components, Energy Conversion and Management, 64 (2012) 213-221.

[47] E.E.B. Gomes, D. McCaffrey, M.J.M. Garces, A.L. Polizakis, P. Pilidis, Comparative Analysis of Microturbines Performance Deterioration and Diagnostics, in: GT2006 - ASME Turbo Expo 2006: Power for Land, Sea and Air, ASME, Barcelona, Spain, 2006, pp. 269-276.

[48] F. Caresana, L. Pelagalli, G. Comodi, M. Renzi, Microturbogas cogeneration systems for distributed generation: Effects of ambient temperature on global performance and components' behavior, Applied Energy, 124 (2014) 17-27.

[49] H. Nikpey, M. Assadi, P. Breuhaus, Development of an optimized artificial neural network model for combined heat and power micro gas turbines, Applied Energy, 108 (2013) 137-148.

[50] H. Nikpey, M. Assadi, P. Breuhaus, P.T. Mørkved, Experimental evaluation and ANN modeling of a recuperative micro gas turbine burning mixtures of natural gas and biogas, Applied Energy, 117 (2014) 30-41.

HOW TO CITE THIS ARTICLE

S. S. Talebi, A. Mesgarpur Tousi, A. Madadi, The Effect of Turbine Blade Erosion on the Gas Path Measurements and Performance of Micro Gas Turbines, AUT J. Mech Eng., 7(4) (2023) 419-438.

DOI: 10.22060/ajme.2024.23057.6099